Experimental Mechanics
DOI 10.1007/s11340-015-0023-3

A Methodology for Characterizing the Interfacial Fracture Toughness of Sandwich Structures using High Speed Infrared Thermography

W. Wang[1] · **J.M. Dulieu-Barton**[1] · **O.T. Thomsen**[1]

Received: 7 October 2014 / Accepted: 6 April 2015

Abstract An experimental method is proposed for obtaining the fracture toughness of an interfacial crack in sandwich structures. The method relates the interfacial fracture toughness with temperature change developed at the crack front. The focus of the paper is the development of an experimental approach that uses high speed infrared (IR) thermography to capture the temperature evolution during the crack growth. The feasibility of using IR thermography is demonstrated on sandwich structure specimens with E-glass/epoxy face sheets and cross-linked PVC H100 foam core loaded in mixed-mode bending. Different crack propagation paths, in the foam core and at the face sheet/core interface are considered. It is shown that IR thermography with 15 kHz frame rate is able to make a quantitative measurement of the crack front temperature associated with the crack growth. A constant of proportionality ψ is derived between the temperature change per unit area at the crack front and the fracture toughness provided by a validated FE model. It is shown that ψ obtained from specimens with the same crack propagation path is identical, even though the specimen dimensions and loading mode-mixities are different. Thus, it is demonstrated that for a particular interface, once ψ is obtained from a known loading condition, the interfacial fracture toughness from any loading configuration can be determined from a direct temperature measurement.

Keywords Fracture toughness · High speed infrared thermography · Mixed mode fracture · Sandwich structures

✉ J. M. Dulieu-Barton
janice@soton.ac.uk

[1] Faculty of Engineering and the Environment, University of Southampton, Southampton, UK

Introduction

Sandwich structures consisting of a thick, low density core material sandwiched between two thin and high stiffness face sheets are used in a wide range of applications such as wind turbine blades, as well as lightweight naval and aerospace structures [1, 2]. Compared to monolithic structures or laminated composites, sandwich structures are well known for their superior bending stiffness and strength to weight ratios as well as their superior stability characteristics. An important damage type found in sandwich structures is debonding between the face sheets and core. Debonds can initiate from manufacturing defects as well as in-service overload or impact. The existence of debonds can cause a significant reduction of the load carrying capacity of sandwich structures as the ability to transfer shear stresses between the face sheets and the cores is compromised. As a result the debonded area will often tend to expand progressively during service lifetime until catastrophic failure occurs [3]. It is therefore important to determine the effect of debonding on the residual strength of the structure.

An important parameter that controls the propagation of debonds is the interfacial fracture toughness, G_c. It is generally recognized that G_c is strongly dependent on the relative amount of mode I and mode II loading (i.e. mode-mixity) applied at the crack tip [4]. The consequence of this dependence is that the complete distribution of G_c under different mode-mixities is required for characterising the fracture behaviour. Furthermore, previous work [5] has shown that the value of G_c also depends strongly on the initial debond tip location (i.e. the debond tip occurs either at the face sheet/core interface, in the face or in the core). Thus, to achieve a thorough understanding of the interfacial fracture behaviour, it is important to characterize G_c for different debond tip locations.

Published online: 28 April 2015

In recent years considerable effort has been targeted at developing methods for characterizing G_c over a wide range of mode-mixities. Quispitupa *et al.* [6, 7] introduced the mixed mode bending (MMB) test method to sandwich structures, which enables the interfacial fracture toughness to be characterized under different loading mode-mixities. In their work both analytical solutions and finite element (FE) models were developed for determining the interfacial fracture toughness. G_c derived from the analytical solutions showed good agreement with the FE results. However, the derivation of generally valid analytical solutions for G_c for sandwich materials is generally complex and possibly elusive due to the complex loading configuration and specimen geometry. Thus, the analytical solution developed in [6] was only valid for sandwich structures containing isotropic material constituents for face sheets and core material. Li and Carlsson [8] developed the tilted sandwich debond (TSD) method for the study of the multi mode interfacial fracture toughness. In this case it was necessary to make an FE model of the TSD specimen to determine G_c, as an analytical solution was not available.

The purpose of the work described in the present paper is to develop an experimental method that enables the characterization of G_c by measuring increases in temperature at the crack front during crack propagation. The method is based on the use of infrared (IR) thermography [9] for capturing the crack front temperature. Compared to traditional single point measurement sensors such as thermocouples, IR thermography allows the surface temperature to be measured in a non-contact manner with high spatial and temporal resolutions. As the interfacial fracture toughness is derived directly from the measured temperature value, the method does not require knowledge of the global response of the test/rig/specimen and can be applied to different loading conditions.

A significant challenge associated with the temperature measurement is that, there is rapid heat dissipation at the newly created fracture surfaces as the crack front progresses. Furthermore the crack propagation can be very fast, especially in brittle materials, so a high frame rate is required to measure the temperature at the crack front. For example, it has been shown in [10] that the crack propagation velocity in PMMA materials can be higher than 200 m/s at loading rates of less than 0.5 mm/min. Thus, to capture the short-lived temperature increase during crack growth, IR thermography must be employed with very high recording rates (i.e. frame rates). Modern IR detectors, such as the one used in this work (Cedip Silver 480 M photodetector), provides a maximum frame rate of 383 Hz when using the full detector array. By reducing the window size (i.e. using a subset of the full detector array) the achievable frame rate can be increased up to 16 kHz (corresponding to 64×12 elements of the detector array). A further consideration is that to avoid image blurring, shorter integration times (i.e. exposure times) are necessary meaning that the detector collects fewer photons, thereby reducing the detector output signal, hence increasing the contribution of detector noise and reducing thermal resolution. Thus, for current IR detectors, a compromise is required between the data recording rates, the field of view and the thermal resolution. The present paper describes the feasibility of using IR thermography at 15 kHz frame rate to capture the crack surface temperature during fracture. Since the standard temperature calibration curves provided by the manufacturer are not valid for the frame rates in the kHz region and the necessary short integration times, a bespoke calibration process for high speed thermography developed in [11] was used to achieve a quantitative temperature measurement. Therefore a key objective of the work is to demonstrate that the high speed IR thermography can be used to capture the temperature evolution at the crack front during fracture, which again can be used directly for determining the interfacial fracture toughness for sandwich structures.

Firstly, the methodology and the experimental setup for obtaining the crack front temperature associated with crack growth are introduced. The feasibility of the methodology is then examined by obtaining the interfacial fracture toughness of sandwich structures loaded in the MMB test fixture [6, 7]. The MMB loading configuration was used because it is a well-established method which enables investigations of mixed mode interfacial crack propagation. Sandwich specimens containing cross-linked PVC foam core and glass fibre reinforced composite face sheets are studied.

Methodology

Characterization of Material Fracture Toughness

Fracture in solids occurs when the potential energy stored at the crack tip is large enough to overcome the energy required to create new surfaces [12]. The fracture toughness, G_c, is a parameter that defines the required energy for an increment of crack extension in a unit area [13]:

$$G_c = -\frac{dW_s}{dA} \tag{1}$$

where W_s is the energy required to create new surfaces and A is the area of the crack increment.

During the fracture process part of the potential energy (stored during elastic deformation) is consumed by the plastic deformation at the crack tip, while the rest of the energy is dissipated as heat. According to the first law of thermodynamics, the work required to create new surfaces can be described as:

$$W_s = -(W_p + Q) \tag{2}$$

where W_p is the plastic work and Q is the heat released during fracture process.

For ductile materials, plastic deformation is induced ahead of the crack tip which results in almost all the potential energy being consumed by plastic work [14]. Previous work has shown the majority part of the plastic work is converted into heat, amounting to nearly 90 % in metals [15] and 60 % in polymers [16]. For brittle materials like glass and ceramics, the plastic deformation at the crack tip is negligible and almost all the potential energy is dissipated as heat released during the fracture process [12]. Fig. 1 illustrates the generated heat at the crack front (the grey dashed line area) associated with a crack advance of length a. During fracture, heat is generated at the newly created crack surface (the area with length a and width b) as well as into the region below the crack surface with depth t according to the material thermal diffusivity. As two crack surfaces are created during the fracture process, heat is generated in two volumes (V_1 and V_2) and can be evaluated from:

$$Q = \rho C\left(\int_{V_1} \Gamma(V_1)\mathrm{d}V_1 + \int_{V_2} \Lambda(V_2)\mathrm{d}V_2 \right) \tag{3}$$

where ρ is the material density, C is the specific heat, and Γ and Λ are functions of temperature change related to the dimensions of the two crack volumes.

To simplify the expression in Eq. (3), the integral terms in the bracket are notated together as ΔT_V in the following treatment. By substituting Eq. (3) into Eq. (2) and then into Eq. (1), the fracture toughness can be related to the increase in temperature at the crack front as:

$$G_c = \frac{W_p + \rho C \Delta T_V}{2\Delta A} \tag{4}$$

As described above, when considering the fracture in brittle or semi-brittle materials two assumptions can be made: 1) the plastic deformation at the crack tip is highly localised and very small; 2) the heat generated in the area below the crack surface is small and negligible. Since the foam core material considered in this investigation is a cross-linked PVC foam which is generally considered as brittle [17, 18], the two assumptions stated above can be adopted. Accordingly, it is possible to reduce Eq. (4) so that the material fracture toughness can be expressed through the following proportionality:

$$G_c = \psi \frac{\Delta T_S}{\Delta A} = \psi \frac{\Delta T_S}{a \times b} \tag{5}$$

where ΔT_S is the integral of temperature over the two crack surfaces and ψ is a constant of proportionality with units of J K^{-1} m^{-3}.

It can be seen that Eq. (5) provides a simple linear relationship between fracture toughness and temperature, without recourse to knowledge of the applied load or displacement in a test. Accordingly, by experimentally determining ψ for different materials, it is possible to derive the material fracture toughness simply from a direct temperature measurement in any loading configuration. The shortcoming is that to determine ψ, G_c must be known for given interfacial materials. It is proposed that G_c is determined from a validated FE model (or analytical model if available) for a well-defined test configuration and used in Eq. (5) to obtain ψ. Once ψ is known for given interfacial materials then the temperature measurement alone can be used to determine G_c for any test configuration and mode-mixity.

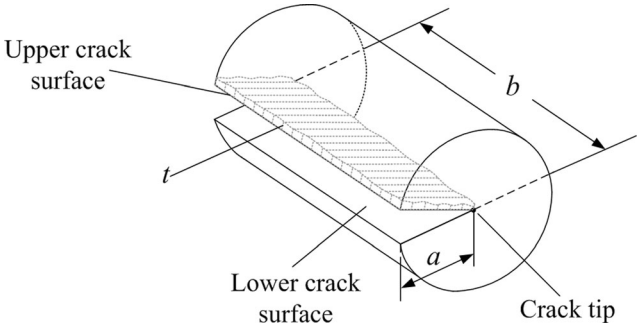

Fig. 1 Temperature increase at the crack front during crack propagation

The possibility of using Eq. (5) to determine the fracture toughness was studied by measuring the temperature change at the crack tip of the face sheet/core interface of a sandwich specimen. Figure 2 shows the experimental methodology that was devised to obtain the temperature change per unit area, i.e. $\Delta T_S / \Delta A$ in Eq. (5). The adopted experimental procedure is as follows:

1. The sandwich structure (specimen) that contains an initial debond is loaded statically until a pre-manufactured debond starts to propagate.
2. An IR detector captures the temperature change associated with crack growth across the entire crack front.
3. A high speed camera is used to capture the crack advance by taking white light images from the side of the specimen. Thus, the crack increment area (ΔA in Eq. (5)) can be obtained by multiplying the crack advance a by the specimen width b.

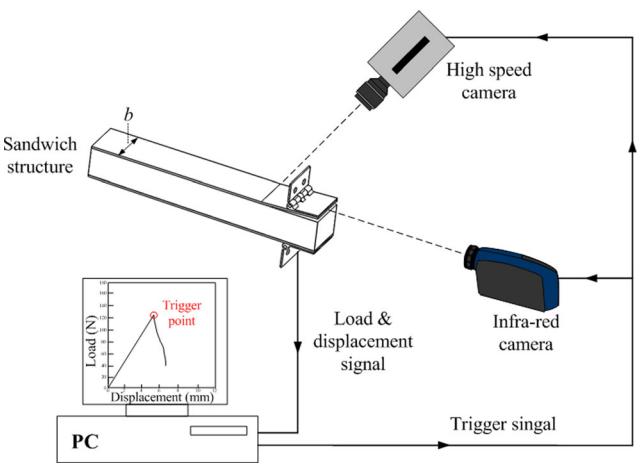

Fig. 2 Test setup for measuring temperature change per unit area at the crack surface

4. The load and displacement data from the test machine are collected and analysed in real-time using a LabView program. When the load starts to decrease the program sends a trigger signal to both IR and high speed cameras to initiate data capture.
5. The cameras are set up in pre-trigger mode and are continuously capturing data. When the trigger signal is received IR images captured within 6 s before and after crack propagation are recorded.

High Speed Infrared Thermography and Temperature Measurements

The IR detector system used in this work is a Cedip Silver 480 M IR camera that contains a photo detector that is sensitive to radiation with wavelengths from 3 to 5 μm. The detector comprises a 320×256 element indium antimonide (InSb) detector array. The output from the detector array is presented as a 14 bit digital level (DL) bitmap. When using the full detector array the maximum available frame rate is 383 Hz. The frame rate can be increased by decreasing the size of the image (i.e. number of detector elements). To maintain a 'full-field' measurement at the crack front, a frame rate of 15 kHz was selected in this work as this leads to a reasonable array size of 64×12 pixels.

The conversion of the detector DL into temperature normally requires two steps: the temperature calibration of the detector array and the determination of the surface emissivity of the objects. A calibration is necessary that relates the temperature to the detector DL output which is provided by the manufacturer for given integration time. Since each detector element possesses its own behaviour, the response of each element must be corrected relative to the mean response of the array. This step is called the non-uniformity correction (NUC) and is based on a linear relationship between the detector digital output and the incident radiation. The gain and offset of each detector element is provided by the NUC so that response from each detector element is uniform. At high frame rates such as 15 kHz used in the current work, the integration time is very small (e.g. 60 μs at 15 kHz) which decreases the photon emittance available for measurement significantly and results in a very low detector DL output, hence this is outside the range of standard calibrations supplied by the manufacturers. In such a case the linear response of the detector cannot be assumed, and therefore the standard NUC procedure is also not appropriate for high speed IR thermography. A calibration approach for high speed thermal imaging has been developed in [11]. According to this approach, the calibration is performed for each detector element individually across the array (64×12 pixels), thereby addressing the problems of image non-uniformity and detector nonlinearity in a single step. In [11], the calibration approach has been experimentally validated using the same IR camera system as used in this work. Thus, the developed calibration approach for high speed thermography was adopted in this work.

Table 1 Detector precision at 15 kHz frame rate [11]

Temperature (°C)	Sensitivity (°C/DL)	Precision (°C)
15	0.14	0.32
20	0.11	0.27
35	0.08	0.19
45	0.06	0.14

The emissivity of an object must be known to accurately apply the above procedure. When estimating the surface emissivity at the crack surfaces, it is possible to treat the crack surface area as a V-groove cavity as shown in Fig. 3 (a), where δ and a represent the crack opening distance and the crack increment, respectively. Thus, the effective emissivity (e_0) of the cavity can be estimated as follows [19]:

$$e_0 = \frac{e\left[1+(1-e)\left(\frac{\delta}{\delta+2a}-\sin^2\left(\frac{\theta}{2}\right)\right)\right]}{e\left(1-\frac{\delta}{\delta+2a}\right)+\frac{\delta}{\delta+2a}} \tag{6}$$

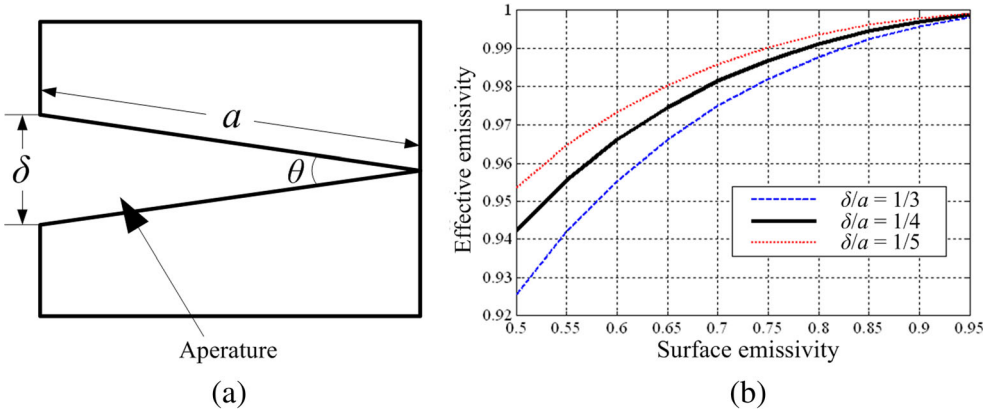

Fig. 3 **a** V-groove cavity geometry with: crack opening distance δ, vertex angle θ and crack increment a; **b** Cross-linked PVC foam core material: effective emissivity vs. material surface emissivity values for different δ/a values

Table 2 Material properties of composite face sheets and H100 PVC foam core [20]

Materials	Young's modulus (E_x)	Young's modulus (E_y)	Shear modulus (G_{xy})	Poisson's ratio (ν_{xy})
Core	56 MPa	128 MPa	32 MPa	0.2
Face sheet	17 GPa	–	7.26 GPa	0.17

where e is the surface emissivity of the cavity material, and θ is the vertex angle of the groove. Figure 3 (b) plots the effective emissivity against the material surface emissivity values for different δ/a values (with θ calculated correspondingly by the law of cosines).

From the experimental results conducted in this work, a δ/a value of about ¼ was commonly observed for all the test specimens (estimated from the dimensional data collected in the white light images). As shown in Fig. 3 (b), for the composite and PVC foam materials used in this work, it is reasonable to assume that the apparent emissivity at the crack surface is close to that of the blackbody with the value of 1.

For an accurate temperature measurement, the camera and objects must be isolated from any reflections of the environment. This is achieved by draping a black curtain around the test area. Moreover, the measurement must take the detector noise (i.e. measurement precision) into account as this affects the lower limit of the temperature that can be assessed. For an integration time of 1300 μs, the IR detector used in this work provides a sensitivity of 4.2 mK/DL and a detector noise of 17 mK at 25 °C. However, at high frame rates, the detector noise increases as the integration time decreases. An assessment of the measurement precision at a 15 kHz frame rate of the camera was provided in [11] and is given in Table 1. The sensitivity represents the temperature increment per DL and the precision is the detector noise calibrated into °C (the detector pixel standard derivations obtained from 20 readings at identical temperature). A lower precision can be seen in the Table compared to that with longer integration time.

Experimental Arrangements

Test Specimens and Materials

The sandwich specimens studied in the current work consist of Divinycell H100 cross-linked PVC foam cores and 210 gm^{-2} plain woven E-glass/epoxy composite face sheets. Firstly, sandwich panels were manufactured in a single shot resin infusion process using Prime 20 LV epoxy resin by Gurit. The mechanical properties of the sandwich constituent materials are listed in Table 2 [20]. During the manufacture, a thin Teflon film of 25 μm thick was placed between the face sheet and the core to create an initial debond region across the width of the panel.

Test specimens were cut from the panels and tested using the MMB test rig shown in Fig. 4. The rig was loaded by a downward force, P, introduced through the loading yoke, and transferred to the beam specimen via roller and steel hinges. Hinges were bonded on the specimens using an Araldite^{TM} epoxy resin cured for 12 h at room temperature. The MMB rig allows variation of the loading conditions between mode I (tensile normal) and mode II (sliding shear) mainly by changing the lever arm distance, c, and the core thickness, t_c [6]. For instance, mode I dominated loading can be applied at the crack tip by using a large lever arm distance and a high core thickness. The increase of the face sheet thickness (t_f) or decrease of the span length (L) also promotes a mode I dominated loading.

The constant of proportionality, ψ, given in Eq. (5) was obtained under different loading modes by changing the constituent material dimensions and loading configurations to develop different G_c values for each specimen. A summary of the dimensions and loading conditions of the test specimens is

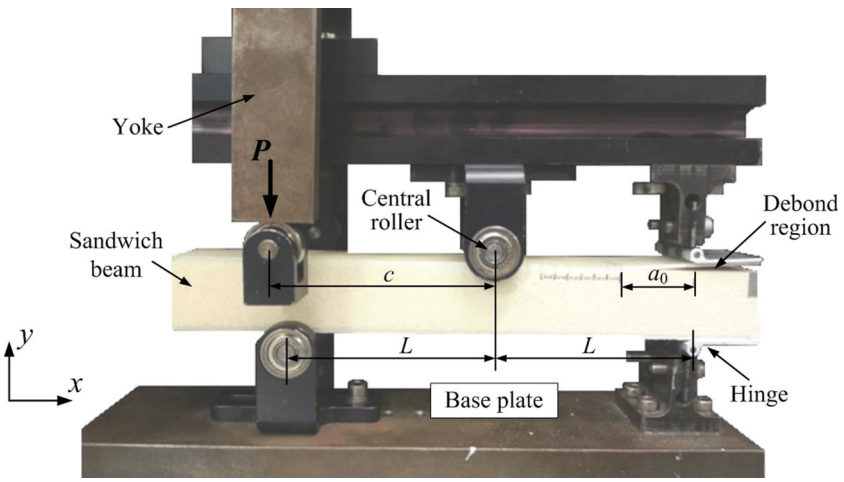

Fig. 4 Sandwich beam specimen with initial debond loaded in the MMB test rig

Table 3 The dimensions and loading conditions of different test specimens (SD not included as they were less than 0.033 mm in all cases)

Specimens	S1	S2	S3	S4	S5	S6	S7	S8	S9	S10	S11
t_f (mm)	1.68	1.69	1.70	1.70	1.87	1.91	1.51	1.52	1.50	1.51	1.49
t_c (mm)	25	25	25	25	15	15	15	15	15	15	15
b (mm)	28.83	31.30	31.27	30.02	30.09	30.09	29.58	29.47	29.60	29.52	29.68
a_0 (mm)	28.12	27.48	23.51	28.50	26.03	26.44	24.47	25.21	23.30	26.89	24.61
$2\ L$ (mm)	150	150	150	150	160	160	150	150	150	150	150
c (mm)	65	50	50	50	45	45	40	40	55	55	55

shown in Table 3. The specimen dimensions and initial crack length are average values taken from 5 measurements; in all cases the standard deviation (SD) was less than 0.033 mm. Furthermore, the applied loading modes also influence the crack propagation path (e.g. the crack can propagate either in the core, face sheet or at the face sheet/core interface) [7, 21]. The aim is that the test specimens generate different crack propagation paths to allow different interfacial conditions to be evaluated.

Experimental Setup

Sandwich specimens mounted in the MMB rig were tested in an Instron ElectroPuls machine (E1000) with a 1kN actuator and load cell capacity. The load cell is calibrated by the manufacturer and has a quoted accuracy of±0.5 % [22]. The actuator/load cell was connected to the loading yoke and a compressive load was applied to the MMB test fixture. The specimens were loaded at a rate of 1 mm/min.

The crack front of the specimen viewed by the IR camera is shown in Fig. 5. The reduced detector array at 15 kHz results in a small field of view which is indicated by the yellow rectangular area in the middle of the image. To enable the temperature measurement across the entire crack front, the small field of view must be positioned properly. As indicated in the image, for the measurement of each specimen, the detector focal length is adjusted to allow the length of the rectangular area to be the same as the width of the specimen and the rectangle is positioned just above the foam core. This arrangement enables the crack front temperature to be measured with maximum spatial resolution. The metal tape shown in the image is bonded to the foam core surface to highlight the edge of the core and the area of the crack front. Before the measurements, the IR camera is rotated 15° down relative to the horizontal plane so that the upper and lower crack surfaces at the crack front can be observed. Together with the IR images, the corresponding load data output from the test machine is recorded by the IR camera system at 15 kHz, hence the collected load data has the units of DL. To obtain the crack increment area (ΔA), the crack advance is measured using a Photron SA-3 high speed camera with a frame rate of 5 kHz. A lower frame rate is acceptable for the high speed camera than for the IR camera because the crack length was determined from two stationary points between the initial crack tip and the crack tip after fracture. The white light images obtained from the high speed camera were calibrated using a pre-applied scale of 15 mm on the specimen surface. To determine the number of pixels over the 15 mm scale, the measurements were taken five times and an average value from these measurements was used for calibrating the image spatial resolution. The image resolutions were approximately 0.026 mm with a SD smaller than 1.414×10^{-4} mm. As the recording capacity of the IR and high speed cameras are limited (only images captured within 6 s can be saved in the memory), a LabView code was designed to trigger image capture of both cameras when the crack propagated. Both cameras were setup so that an equal number of images recorded before and after the triggering were saved to the memory.

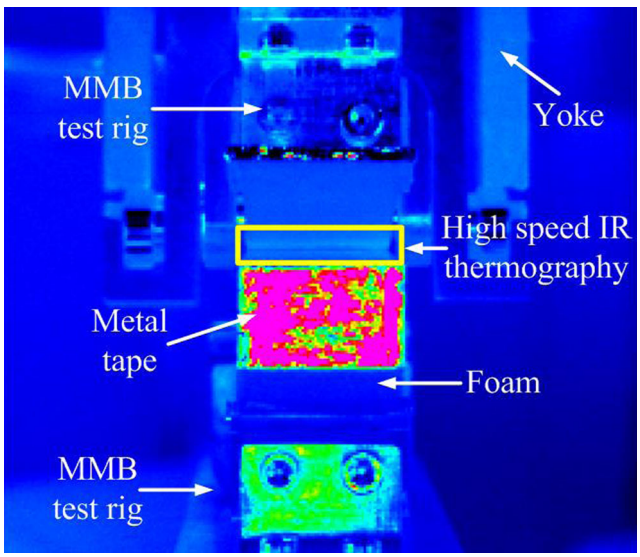

Fig. 5 Crack front viewed by the IR detector and the field of view (*yellow rectangle*) at 15 kHz frame rate

The LabView code acquired the load and cross head displacement from the test machine using a NI USB-6211 analogue to digital data acquisition system with a sampling rate of 10 Hz. When the crack starts to initiate there is a sudden decrease in the applied load as shown in Fig. 6 (a). However, due to the electronic noise, there is not a monotonic increase in

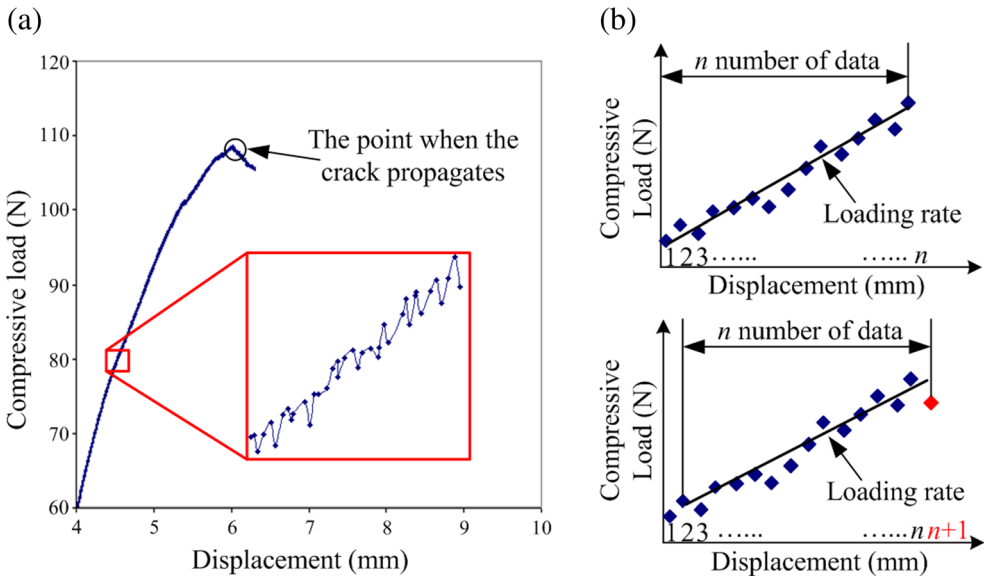

Fig. 6 **a** Load-displacement data collected from LabView code; **b** Derivation of the loading rate

the load signal during the initial loading (see the red zoomed insert in Fig. 6 (a)). Therefore simply using a reduction in the load signal as a trigger is not appropriate; instead the loading rate is used as the trigger to capture data. Figure 6 (b), shows the loading rate can be obtained by performing a linear fit of a straight line over '*n*' number of data points. This means that the crack initiation is identified when the loading rate becomes negative. It is clear that the accurate measurement of the loading rate depends on the choice of the integer '*n*'. If *n* is too small the true trend of the load-displacement curve is not captured. Also if *n* is too large, identification of the crack initiation will be inaccurate. Therefore '*n*' was determined from the load-displacement curve of a pre-tested specimen in which linear fitting was applied using different values of *n* from 5 to 50. When *n* was chosen to be smaller than 10, the derived loading rates did not capture the true load-displacement behaviour of the specimen, because the loading rates were recorded randomly as positive and negative due to the electronic noise. As *n* was incremented in steps of 10 from 10 to 50, it was shown that for $n=20$ and above the turning point of the load displacement curve happened at the same data point. Therefore it was concluded that using a value *n* of 20 provided the most effective identification of the crack initiation.

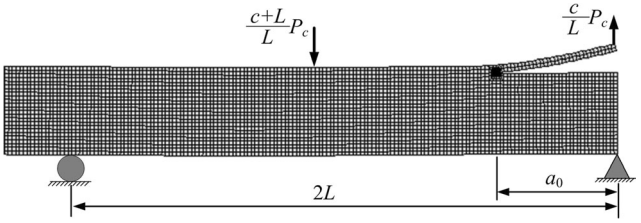

Fig. 7 FE model of the specimens loaded under the MMB loading conditions

FE Analysis

FE analysis was performed to extract the values of the interfacial fracture toughness and the crack tip loading mode-mixity (i.e. the relative amount of mode I and mode II stresses applied at the crack tip) for different specimens. As described by the FE analysis of the MMB specimen in [6], the interfacial fracture toughness G_c can be derived from the relative crack flank displacements using the following expression [23]:

$$G_c = \frac{\pi\left(1+4\varepsilon^2\right)}{8H_{11}|x|}\left(\frac{H_{11}}{H_{22}}\delta_y^2+\delta_x^2\right) \tag{7}$$

where δ_y and δ_x are the opening and sliding relative displacements at a short distance x behind the crack tip, ε is the oscillatory index and H_{11} and H_{22} are the material anisotropy parameters, defined in [24].

Table 4 Fracture test results for different specimens

Specimens	P_c (N)	Crack propagation path	ϕ (°)	G_c (J/m^2)
S1	106.2	Core	−18.16	796.2
S2	159.8	Core	−19.15	886.2
S3	178.7	Core	−19.08	861.2
S4	151.3	Core	−19.72	912.7
S5	188.1	Core	−25.19	657.9
S6	200.8	Core	−25.82	763.2
S7	134.2	Interface	−24.45	519.1
S8	163.7	Interface	−25.38	801.1
S9	112.3	Interface	−21.58	622.0
S10	103.9	Interface	−22.34	688.2
S11	110.2	Interface	−21.92	655.2

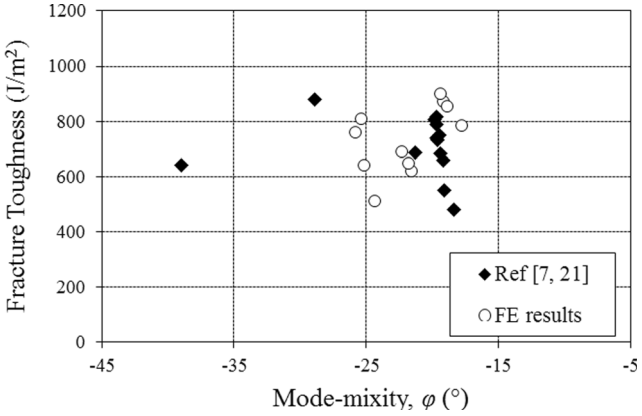

Fig. 8 Comparisons of the fracture toughness values obtained from this work with the values in Ref [7, 21]

The values of δ_y and δ_x in Eq. (7) can be directly extracted from the crack node displacements of the FE model using the loading condition that the critical load (P_c) at the onset of crack propagation is applied.

To quantify the applied loading mode at the crack tip for each specimen, the crack tip mode-mixity (ϕ) can be derived from δ_y and δ_x using the equation below [25, 26]:

$$\phi = \tan^{-1}\left(\frac{\delta_x}{\delta_y}\right) - \varepsilon \ln\left(\frac{x}{h}\right) + \tan^{-1}(2\varepsilon) \tag{8}$$

where h is a characteristic length which is commonly chosen as the face sheet thickness [2, 6]. The value of the mode-mixity ϕ provides a quantitative measure of the relative amount of mode I and mode II stresses applied at the crack tip.

Two dimensional FE models of the specimens loaded in the MMB test rig were developed in the commercial FE package ANSYS 12.1 [27]. The core and face sheet mechanical properties are provided in Table 1. The geometry of the model with the applied boundary conditions is shown in Fig. 7. The MMB loading arrangements were obtained from the static beam analysis [6]. The model uses an eight-node 2D plane strain elements (PLANE 183). A highly refined mesh with a minimum element size of 0.01 mm was used at the crack tip to accurately capture the crack tip displacements. The results of [28] indicate that the G_c and ϕ values derived from a numerical solution will be affected by the displacement oscillations in a very small area near the crack tip. To avoid the oscillatory error, the Crack Surface Displacement Extrapolation (CSDE) method [2] has been used in the previous work [6]. The method derives the displacements, δ_y and δ_x, from the node outside the oscillatory error zone and linearly extrapolates the results to the crack tip. A detailed description of the method can be found in [26, 28].

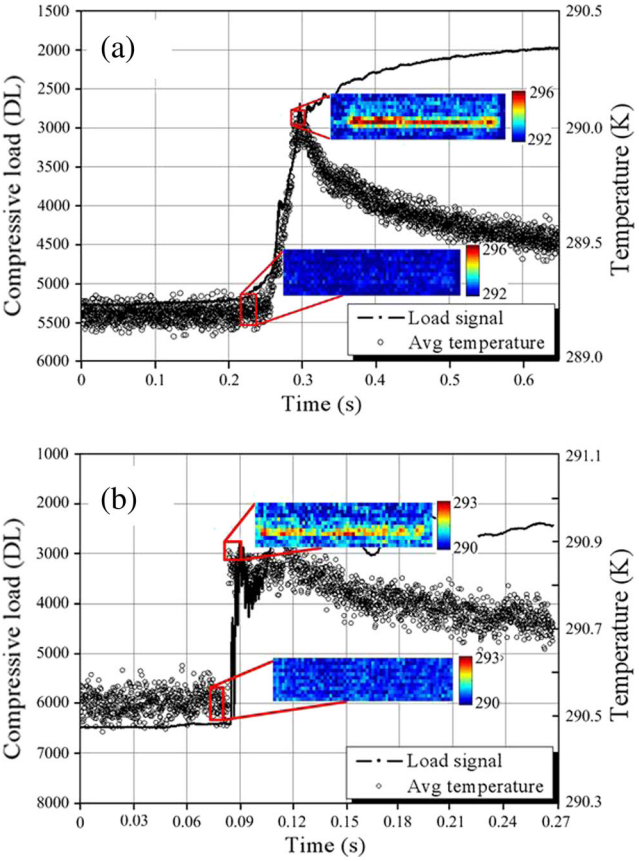

Fig. 10 Load and average temperature trace obtained from specimens with **a** crack propagation path in the core, and **b** crack propagation path at the face/core interface

Fracture Test Results

Specimens with different loading conditions given in Table 3 were tested. The critical load (P_c) for crack propagation and the crack propagation paths observed form the fracture tests are summarized in Table 4. For each specimen, the applied crack tip mode-mixity ϕ and the interfacial fracture toughness

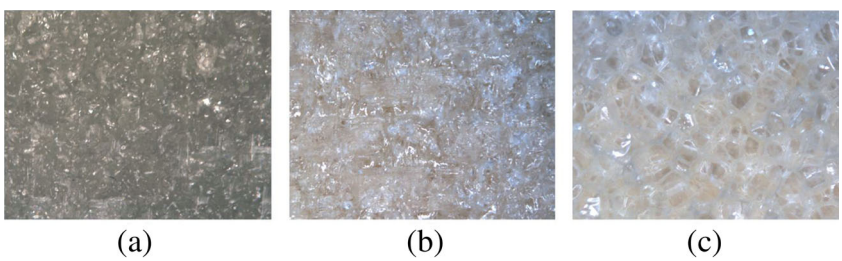

Fig. 9 **a** Crack surface on the face sheet side, **b** Crack surface on the core side, **c** Surface texture of the foam

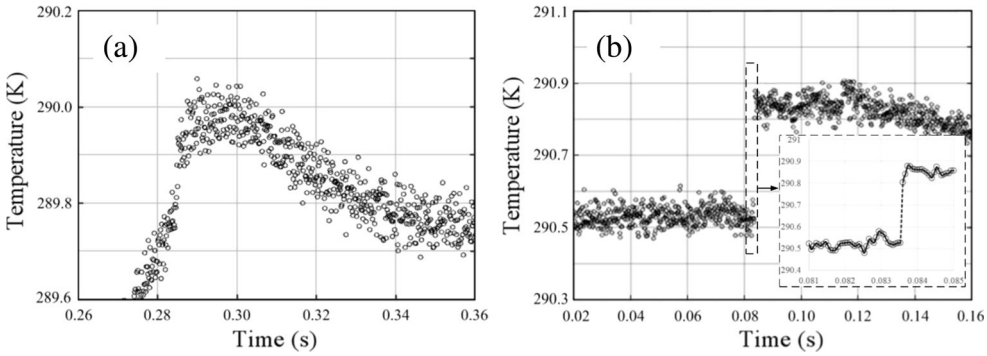

Fig. 11 Close-up of the average temperature trace with: **a** corresponding to Fig. 10 (a) and (b) corresponding to Fig. 10 (b)

G_c were calculated from the FE models. The values of G_c obtained in this work are compared with the results shown in [7, 21] (see Fig. 8), where sandwich specimens with PVC H100 foam core and E-glass/polyester composite face sheets were tested using the MMB test rig. Figure 8 shows that the results obtained here correspond reasonably well to those reported in [7, 21].

Two different crack propagation paths were observed. When the specimen was subjected to a mode I dominated loading (small magnitude of ϕ), the crack propagated in the foam core just below the face sheet/core interface. As ϕ increases the crack tended to propagate at the face sheet/core interface. This can be attributed to the increased negative shear stresses acting at the crack tip that forces the crack to propagate along the interface. The observed crack propagation paths for the different loading mode-mixities agree well with results reported in [7].

When the crack propagation path is at the bi-material interface, the crack surface may contain different material constituents, and this makes the proportionality between G_c and temperature change, defined as ψ in Eq. (5), questionable. The constituents on the fracture surface from both sides of the interface were inspected post-mortem. Figure 9 shows microscopic images of the fracture surfaces that indicates an interfacial crack propagation path. The fracture surface on the face sheet side shows a resin surface texture without any foam attached. For the fracture surface on the core side, open foam cells (see Fig. 9 (c)) can be observed. These are (at least partially) covered by a resin layer, which indicates that the interfacial crack was propagating along the resin layer between the face sheet and core. Thus it is theorized that Eq. (5) is valid also for the specimens displaying interfacial crack propagation paths.

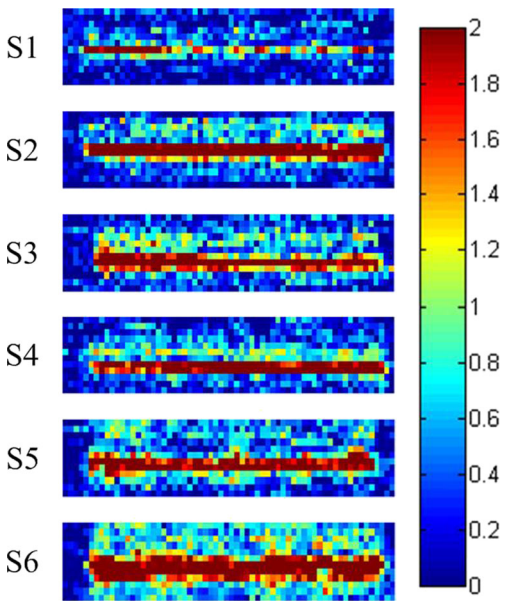

Fig. 12 ΔT images obtained from specimens with the crack propagation path in the core

Characterization of Interfacial Fracture Toughness

Temperature Field Associated With Crack Propagation

The temperature change associated with the crack growth was studied by correlating the thermal data captured at the crack front with the load signal. Figure 10 plots the average temperature value taken across the crack front (i.e. the yellow

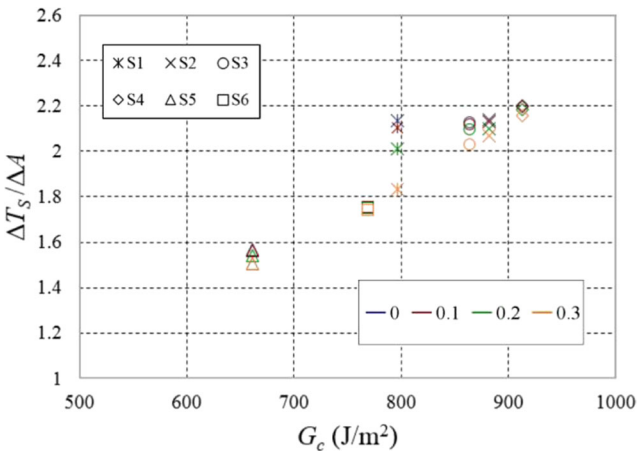

Fig. 13 $\Delta T_s/\Delta A$ against the fracture toughness obtained from different threshold values (0, 0.1, 0.2 and 0.3) for specimens with crack paths within the foam

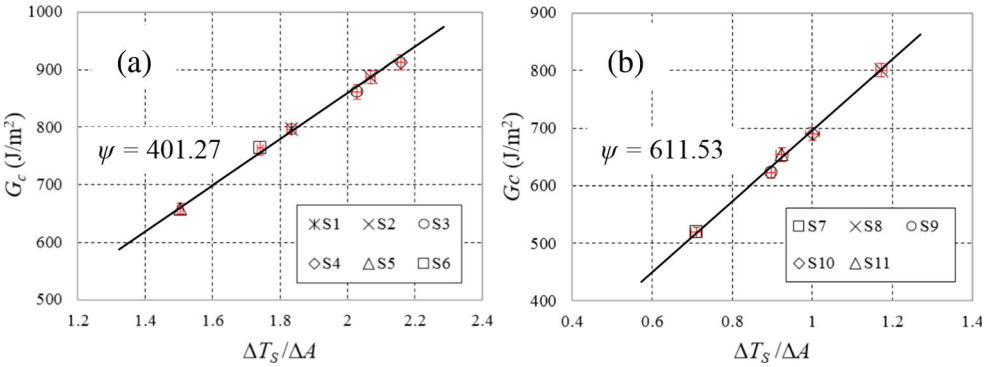

Fig. 14 $\Delta T_s/\Delta A$ against fracture toughness for specimens with **a** cracks paths in the core, and **b** crack paths along the face sheet/core interface

rectangular area in Fig. 5) obtained from two specimens (S3 and S11) with different crack propagation paths. The corresponding load trace in DL shown in the plots was collected simultaneously with the temperature by directly connecting the analogue output of the test machine to the IR camera system and recording alongside the IR output. As a specimen was loaded under displacement control, the decrease of the compressive load shown in the plots indicates that the crack started to propagate. From the temperature trace obtained form different crack propagation paths, an increase of the average temperature value can be observed at the time when the compressive load starts to decrease. This clearly indicated that the increase of the temperature at the crack front was caused by the energy release associated with the crack growth. In both plots, the average temperature values observed before the crack propagation vary within the range about 0.1 °C which can be attributed to the detector noise. As some heat must be dissipated during plastic deformation, and as there is little or no increase in temperature prior to the crack initiation, the temperature trace in Fig. 10 provides the evidence that the plastic deformation at the crack tip is very small. Hence the assumption of negligible plastic deformations made in deriving Eq. (5) is confirmed. A close-up of the average temperature value shown in Fig. 10 is plotted in Fig. 11 from which it is observed that a large number of data points were collected close to the maximum average temperature value before the temperature started to decrease. This indicates that the 15 kHz frame rate used in this work was capable of capturing the temperature increment before the heat dissipated. In Fig. 11 (b) the sudden change in the average temperature trace indicates that the crack was propagating very fast. Here only 2 data points were sampled before the average temperature reached the maximum value (see the small window in Fig. 11 (b)). Thus demonstrating the necessity for high speed IR image capture to obtain the crack front temperature trace.

In Fig. 10 thermal images before and after crack propagation are plotted. The red rectangular temperature maps shown in each plot represent the following: the thermal image before crack propagation was obtained as the average of 100 thermal images collected just before the crack growth, and the thermal image at the time when the average temperature reaches the maximum value showing the crack front temperature after crack growth. The thermal images show a clear temperature increase at the crack front immediately after the crack propagation has occurred. The temperature difference between the two thermal images before and after crack propagation gives the temperature change image (ΔT image) from which the overall temperature increase at the crack front (i.e. ΔT_S in Eq. (5)) can be obtained. Fig. 12 shows examples of the ΔT images obtained from the specimens with the crack propagation path occurring within the core. Thus, the overall temperature increase collected at the crack front (ΔT_S) can be obtained as the sum of the ΔT values in the image.

Determination of Interfacial Fracture Toughness

In Fig. 12 the temperature increase obtained in specimen S1 is seen to be relatively small compared to those obtained in the other specimens. It has been described in High Speed Infrared Thermography and Temperature Measurements that the IR detector provides a thermal resolution (detector noise) about 0.3 °C at 15 kHz. This means that the detector noise may influence the accuracy of the ΔT value when the temperature/detector output is small. For specimen S1 the ΔT values were mostly in the range from 0 to 0.6 °C, which is close to the detector noise level. Therefore, the accuracy of the ΔT value can be largely influenced by the noise introduced during the measurements. To demonstrate the influence of the noise on the temperature change value obtained at the crack front, a threshold with values from 0 to 0.3 °C was applied to the ΔT images. This means that when the threshold is set to 0.1, ΔT values smaller than 0.1 are set to zero. Figure 13 plots the $\Delta T_S/\Delta A$ values derived from different thresholds against the fracture toughness values for specimens S1–S6. It is shown that, with an increase of the threshold from 0 to 0.3, the $\Delta T_S/\Delta A$ value for specimen S1 decreases significantly, while there is little changes of the $\Delta T_S/\Delta A$ value obtained from other specimens. A similar investigation was also applied to the specimens where an interfacial crack propagation path was observed, and the results obtained were almost identical. Based on the analysis, it is shown that the influence of the detector noise to the ΔT_S value can be minimised for the

current test by applying a temperature threshold of 0.3 °C to the ΔT image.

Figure 14 plots the fracture toughness determined for each specimen against the $\Delta T_S/\Delta A$ values using the 0.3 °C temperature threshold. For specimens with different crack propagation paths, the results were plotted separately as the crack surface has different material properties. For each specimen, the relationship between the $\Delta T_S/\Delta A$ and G_c determines the constant of proportionality ψ described in Eq. (5). The vertical error bars indicate the measurement errors that might be introduced during the tests in determining G_c. The errors considered here include those generated as a result of the measurement errors of the specimen dimensions and crack lengths as well as the accuracy of the load cell readings. Accordingly, the range of the errors for G_c shown in Fig. 14 was calculated based on the SD of the measurements and the accuracy of the load cell readings. The errors that might be introduced in the $\Delta T_S/\Delta A$ calculation include the calibration of the high speed images, the estimation of the crack tip location and the measurement of the specimen width. From the high speed images, the crack tip location was estimated to be within one pixel resolution i.e. 0.026 mm. The SD of the calibrated pixel resolution is smaller than 1.414×10^{-4} mm. Thus, the horizontal error bars shown in Fig. 14 indicate the error in obtaining the crack progression and the SD of the specimen width measurements.

By linear fitting of the data points obtained from the specimens in each plot, a straight line can be obtained which shows that the values of ψ obtained from the same crack surface materials are identical, even though the mode-mixities are different. For the crack surface studied in this work, two values of ψ were determined, one representing crack propagation in the PVC core material, ψ=401.27 J K^{-1} m^{-3}, and one corresponding to face sheet/core crack propagation, ψ= 611.53 J K^{-1} m^{-3}. As specimens were tested with different dimensions (e.g. the face sheet and core thickness) and loading conditions between mode I and mode II, it is shown that the influences of the specimen dimensions and loading conditions on ψ are insignificant. This is expected as ψ directly relates the heat generated at the crack surface with the fracture energy. Thus, the values of ψ obtained in the results can be used to determine the fracture toughness in different loading configurations when the fracture surface contains the same materials as those studied in this work.

Conclusions

A methodology has been developed for capturing the temperature increase at a propagating crack using high speed IR thermography. It has been shown that the IR thermography with 15 kHz frame rate was capable of a quantitative measurement of the crack front temperature associated with the crack growth.

It has been proposed that by measuring the temperature alone the interfacial fracture toughness in foam cored sandwich structures can be determined. It is demonstrated that for given sandwich constituent materials, a constant of proportionality ψ can be derived between the measured temperature change per unit area ($\Delta T_S/\Delta A$) and G_c provided by an FE model for different interfaces. Once ψ is obtained from a known loading configuration it can then be used together with the temperature change per unit area ($\Delta T_S/\Delta A$) measured from any loading configuration to give the interfacial fracture toughness for a particular interface.

An initial demonstration of the method is provided for sandwich specimens with a cross-linked PVC H100 foam core and E-glass/epoxy face sheets. Specimens with an initial debond were loaded in a MMB test configuration subjected to different loading mode-mixities. Two different crack propagation paths were observed during the tests: 1) a debond growing in the core material just below the interface, and 2) a debond propagating along the face sheet/core interface. For both crack propagation paths, an increase of the temperature at the crack front associated with the crack growth was captured by the IR camera. For each specimen, the values of ψ were obtained from the relationship between the measured $\Delta T_S/\Delta A$ value and the known fracture toughness G_c obtained from the validated FE model. It was shown that ψ obtained from the specimens with the same crack propagation path was identical. Also, ψ was not influenced by change of the specimen dimensions and loading conditions. Thus, it has been demonstrated that by determining the values of ψ, the fracture toughness can be determined in any test configurations by a direct temperature measurement. Further work is required to fully validate this proposition but the work described in the paper provides an important first step to show that the temperature measurement is possible and indeed feasible with high speed IR imaging, and further that the measured temperature change per unit area ($\Delta T_S/\Delta A$) can be linked directly to the fracture toughness G_c through a simple linear relationship. Moreover the work in the paper paves the way to provide a novel *G*-control approach to fracture testing where the temperature measurement is used to control the test machine. Work is continuing on both of the above possibilities.

Acknowledgments The work presented was co-sponsored by the University of Southampton and the Danish Council for Independent Research | Technology and Production Sciences (FTP), under the research project 'Enhanced Performance of Sandwich Structures by Improved Damage Tolerance' ('SANTOL'). The financial support received is gratefully acknowledged. The foam material supported by DIAB AB Sweden is highly appreciated.

References

1. Zenkert D (1997) An introduction to sandwich construction. EMAS, London
2. Berggreen C (2004) Damage tolerance in debonded sandwich structures, Ph.D. Thesis, Department of Mechanical Engineering, Technical University of Denmark, Denmark.
3. Kulkarni N, Mahfuz H, Jeelani S, Carlsson LA (2003) Fatigue crack growth and life prediction of foam core sandwich composites under flexural loading. Compos Struct 59(4):499–505
4. Liechti KM, Chai YS (1992) Asymmetric shielding in interfacial fracture under in-plane shear. J Appl Mech 59:295–304
5. Li X, Carlsson LA (2001) Fracture mechanics analysis of tilted sandwich debond (TSD) specimen. J Compos Mater 35:2145–2168
6. Quispitupa A, Berggreen C, Carlsson LA (2009) On the analysis of a mixed mode bending sandwich specimen for debond fracture characterization. J Sandwich Struct Mater 76(4):594–613
7. Quispitupa A, Berggreen C, Carlsson LA (2011) Face/core interface fracture characterization of mixed of mixed mode bending sandwich specimens. Fatigue Fract Eng Mater Struct 34(11):839–853
8. Li X, Carlsson LA (1999) The tilted sandwich debond (TSD) specimen for face/core interface fracture characterization. J Sandwich Struct Mater 1(1):60–75
9. Bramson MA (1968) Infrared radiation: A handbook for applications. Plenum, New York
10. Loya JA, Villa EI, Fernandez-Saez J (2010) Crack-front propagation during three-point-bending tests of polymethyl-methacrylate beams. Polym Test 29:113–118
11. Fruehmann RK, Crump DA, Dulieu-Barton JM (2013) Characterization of an infrared detector for high frame rate thermography. Meas Sci Technol 24(10):105403
12. Griffith AA (1920) The phenomena of rupture and flow in solids. Phil Trans R Soc A 221:163–198
13. Irwin GR (1956) Onset of fast crack propagation in high strength steel and aluminium alloys. Sagamore Res Conf Proc 2:289–305
14. Farahmand B (2001) Fracture mechanics of metals, composites, welds, and bolted joints: application of LEFM, EPFM, and FMDM theory. Kluwer, US
15. Taylor GI, Quinney H (1934) The latent energy remaining in a metal after cold working. Proc R Soc A 143:307–326
16. A. Engelter, F.H. Muller, Kolloid Z (1958) 157 (89)
17. Saenz EE, Carlsson LA, Karlsson A (2011) Characterization of fracture toughness (G_c) of PVC and PES foams. J Mater Sci 46(9):3207–3215
18. Maiti SK, Ashby MF, Gibson LJ (1984) Fracture toughness of brittle cellular solids. Scr Metall 18(3):213–217
19. Kelly FJ (1966) An equation for the local thermal emissivity at the vertex of a diffuse conical or v-groove cavity. Appl Opt 5(6):925–927
20. Zhang S, Dulieu-Barton JM, Fruehmann RK, Thomsen OT (2012) A methodology for obtaining material properties of polymeric foam at elevated temperatures. Exp Mech 52:3–15
21. Manca M, Quispitupa A, Berggreen C, Carlsson LA (2012) Face/core debond fatigue crack growth characterization using the sandwich mixed mode bending speicmen. Compos Part A: Appl Sci Manuf 43(11):2120–2127
22. http://www.instron.us/wa/acc_catalog/prod_list.aspx?cid=1165&cname=2580%20Series%20 load%20Cells, accessed in 2014
23. Suo Z (1990) Singularities, interfaces and cracks in dissimilar anisotropic media. Proc R Soc A 427(1873):331–358
24. Østergaard RC, Sørensen BF, Brøndsted P (2007) Measurement of interface fracture toughness of sandwich structures under mixed mode loadings. J Sandwich Struct Mater 9(5):445–466
25. Hutchinson JW, Suo Z (1992) Mixed mode cracking in layered materials. Adv Appl Mech 29:63–191
26. Berggreen C, Simonsen BC (2005) Non-uniform compressive strength of debonded sandwich of debonded sandwich panels-II. Fracture mechanics investigation. J Sandwich Struct Mater 7: 483–517
27. ANSYS 12.1 manual, ANSYS Inc Canonsburg, (2009)
28. Berggreen C, Simonsen BC, Borum KK (2007) Experimental and numerical study of interface crack propagation in foam cored sandwich beams. J Compos Mater 41(4):493–520